nature physics

LETTERS

https://doi.org/10.1038/s41567-020-01150-7

Check for updates

Proton–electron mass ratio by high-resolution optical spectroscopy of ion ensembles in the resolved-carrier regime

I. V. Kortunov[1], S. Alighanbari[1], M. G. Hansen[1], G. S. Giri[1], V. I. Korobov[2] and S. Schiller[1]✉

Optical spectroscopy in the gas phase is a key tool for elucidating the structure of atoms and molecules and their interaction with external fields. The line resolution is usually limited by a combination of first-order Doppler broadening due to particle thermal motion and a short transit time through the excitation beam. For trapped particles, suitable laser cooling techniques can lead to strong confinement (the Lamb–Dicke regime) and thus to optical spectroscopy free of these effects. For non-laser-coolable spectroscopy ions, this has so far only been achieved when trapping one or two atomic ions, together with a single laser-coolable atomic ion[1,2]. Here we show that one-photon optical spectroscopy free of Doppler and transit broadening can also be obtained with more easily prepared ensembles of ions, if performed with mid-infrared radiation. We demonstrate the method on molecular ions. We trap ~100 molecular hydrogen ions (HD^+) within a Coulomb cluster of a few thousand laser-cooled atomic ions and perform laser spectroscopy of the fundamental vibrational transition. Transition frequencies were determined with a lowest uncertainty of 3.3×10^{-12} fractionally. As an application, we determine the proton–electron mass ratio by matching a precise ab initio calculation with the measured vibrational frequency.

The pursuit of increasingly higher resolution in spectroscopy is of fundamental importance in the field of atomic and molecular physics. Techniques such as nonlinear spectroscopy, particle trapping, laser cooling, buffer gas cooling and improved microwave and laser sources have permitted continuous progress in resolution over more than half a century, resulting in major advances in the understanding of radiation–matter interactions and in controlling quantum systems, especially in the optical domain. One key approach to ultra-high (Doppler-free) resolution is the Lamb–Dicke regime (LDR), achieved by confinement of particles, at least in one spatial dimension, to a range substantially smaller than the wavelength of the spectroscopy radiation[3]. Historically, spectroscopy in this regime was first introduced for radiofrequency and microwave spectroscopy for diverse neutral and charged particles. For hyperfine structure spectroscopy of trapped atomic ion clouds, it was already shown in the earliest studies[4] that spectral lines with extremely high quality factors are achievable if the cloud radius is smaller than the wavelength.

For visible radiation ($\lambda\simeq0.5\,\mu$m), the LDR imposes greater experimental challenges, but is today achieved in many experiments. LDR optical spectroscopy has already led to spectacular advances in atomic clock performance (for both atomic ions and neutral atoms)[5–8] and is also an enabling technique for atom-based quantum information processing, cold-atom many-body system studies, and quantum simulations.

For laser-coolable atomic ions, optical LDR spectroscopy has been demonstrated for ion numbers ranging from 1 to 18, arranged in a string[9,10]. For some atomic ion species and most molecular ion species, direct laser cooling is impractical or not possible. One then resorts to the technique of sympathetic cooling. LDR spectroscopy of a single and of two sympathetically cooled atomic ions has been demonstrated, using quantum logic spectroscopy[1,2,11].

For molecules, the LDR has very recently been achieved in a few different configurations: (1) one-photon rotational spectroscopy of molecular ion ensembles at a transition frequency of 1.3 THz (refs. [12,13]), (2) two-photon Raman rotational spectroscopy of a single molecular ion[14], (3) two-photon Raman vibrational spectroscopy (25 THz) of laser-photoassociated diatomic neutral molecule ensembles in an optical lattice trap[15] and (4) two-photon vibrational spectroscopy of molecular ion ensembles, using counter-propagating waves of close wavelength ($\lambda\simeq1.4\,\mu$m)[16]. Some of the line resolutions (defined as the transition frequency divided by the full-width at half-maximum) of up to 8×10^{11} achieved in these works[15] have surpassed the highest values achieved with room-temperature gaseous ensembles and on molecular beams (Methods).

In this Letter, we demonstrate that it is possible to perform ultra-high-resolution one-photon mid-infrared optical spectroscopy of cold ions, on comparatively large and easily prepared ensembles of ions. Although this is demonstrated here on sympathetically cooled ions, it is expected to work also with ions that are laser-cooled directly. The present demonstration is a powerful extension of the previously introduced technique 'trapped ion cluster transverse excitation spectroscopy' (TICTES) from rotational (~1 THz) to vibrational spectroscopy (~50 THz)[12,13]. The technique operates on ion ensembles in a macroscopic linear ion trap and with standard Doppler laser cooling. The crucial aspect is the use of a string-like spatial arrangement of the spectroscopy ions and a spectroscopy radiation with a relatively large wavelength (here 5.1 μm) and propagated at a right angle to the ion trap axis. The technique is to be contrasted with quantum-logic spectroscopy[11,14,17]. Although the latter is powerful and probably extendable to vibrational spectroscopy of molecular ions, its ion preparation technique and the actual spectroscopy procedures are complex and so far restricted to a few specialized research groups worldwide.

In TICTES, two species of ions are simultaneously trapped in a linear ion trap, where one species (LC) is laser-cooled and the other 'target' species (SC) is sympathetically cooled. The corresponding ion numbers are assumed to be $N_{LC}\gg N_{SC}\gg1$. If the two species

[1]Institut für Experimentalphysik, Heinrich-Heine-Universität Düsseldorf, Düsseldorf, Germany. [2]Bogoliubov Laboratory of Theoretical Physics, Joint Institute for Nuclear Research, Dubna, Russia. ✉e-mail: step.schiller@hhu.de

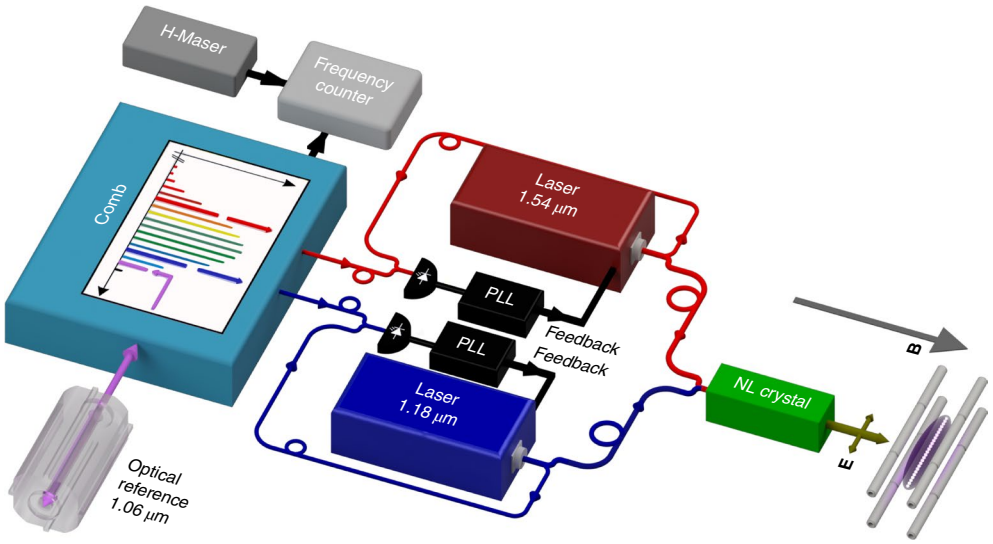

Fig. 1 | Scheme of the key elements of the apparatus. The linear ion trap is on the right. The shape of the two-species Be^+/HD^+ ion cluster is shown. The mid-infrared radiation generated by a nonlinear optical (NL) crystal (olive arrow) propagates perpendicularly to the ion cluster's long axis. The two lasers, L1 (1.18 μm) and L2 (1.54 μm), are phase-locked to two modes of the femtosecond frequency comb (blue and red arrows in the inset diagram on the comb). The comb is phase-locked to a continuous-wave laser (1.06 μm), stabilized to an optical resonator. Only that resonator is shown (bottom left). PLL, phase-locked loop. H, hydrogen.

have charges (q) and masses (m) such that $q_{SC}^2/m_{SC} > q_{LC}^2/m_{LC}$, the species SC will be confined to the region near the trap axis. Here, we focus on a configuration in which the SC ions form an ion string embedded in the LC ion cluster. The dynamics of such a two-species cluster at finite ion temperature has been previously analysed by means of molecular dynamics simulations[12]. The time-averaged spatial distribution of SC ions has a finite width in the radial direction, $\Delta\rho$. For ensembles of HD^+ ions cooled by beryllium ions to a temperature of $T \simeq 10$ mK and arranged in a string-like configuration, $\Delta\rho \simeq 2$ μm was found for our trap parameters in the simulations. A Doppler-free carrier signal with frequency unaffected by ion dynamics was predicted to occur for a spectroscopy wave (λ) irradiation direction transverse to the trap axis (radial direction)[18], assuming that the intrinsic linewidth of the transition is sufficiently narrow. Both numerically and within an approximate analytical model it was furthermore predicted that the strength of the carrier spectroscopy signal decreases continuously from near unity if $\lambda \gg \lambda_c = 2\pi\Delta\rho$ (LDR) to zero for $\lambda \ll \lambda_c$. At $\lambda = \lambda_c$ the carrier signal is 0.5. Whereas in the first experimental investigation the regime $\lambda \gg \lambda_c$ was studied[12], in this work we explore whether a carrier signal is still observable for a small spectroscopy wavelength, $\lambda \simeq 5.1\,\mu\text{m} < \lambda_c$. At this wavelength, the carrier signal strength is predicted to be less than 0.02 under the conditions assumed above[12]. We note that in microwave spectroscopy of trapped atomic ion ensembles, ultra-high resolution of the carrier transition has been observed in the non-LD regime[4,19–22].

Wavelengths of 5 μm and longer permit addressing fundamental and/or first overtone vibrational transitions of most molecular ions, except for hydrides. Such vibrational transitions have natural linewidths in the range from 10 Hz in heteronuclear molecules to nanohertz in homonuclear diatomics. Attainment of the resolved carrier regime can in principle take advantage of these small linewidths to provide, for example, a high spectral resolution of hyperfine structure, a high sensitivity in the study of frequency shifts caused by interaction with externally applied fields and precise measurements of transition frequencies.

To achieve a thorough exploration of the technique's potential in terms of the resolution and accuracy required, we developed an appropriate laser source with ultra-narrow spectral linewidth, ultra-high long-term absolute frequency stability and precise frequency calibration. In the mid-infrared spectral range, such sources are not routinely available. Our source is based on the generation of difference-frequency radiation ($\lambda \simeq 5.1$ μm) from two individually frequency-stabilized, commercial semiconductor lasers ($\lambda_1 = 1.18$ μm, $\lambda_2 = 1.54$ μm) (Fig. 1). We compute the frequency of the mid-infrared radiation from the two laser frequencies, which we measure using a near-infrared frequency comb. Figure 2 presents data on the spectral purity and frequency stability of our source. We estimate the linewidth of the 5.1 μm radiation to be less than 100 Hz (Methods).

Our test ion is the one-electron diatomic molecular ion HD^+ of mass 3 u. The choice of this ion was made due to the feasibility of the ab initio calculation of transition frequencies, so that the experimentally assessed spectroscopic accuracy of the method can also be independently verified. The ab initio calculation method itself has been stringently tested by a recent related experiment in the same ion trap[13]. We interrogate the electric-dipole-allowed, one-photon fundamental vibrational transition $(v = 0,\ N = 0) \rightarrow (v' = 1,\ N' = 1)$ in the ground electronic state ($^2\Sigma_g^+$). v and N denote the rotational and vibrational quantum numbers, respectively. The transition frequency is $f \simeq 58.6$ THz. Details are provided in the Methods.

HD^+ possesses hyperfine (spin) structure and we focus on two transition components, denoted by line 12 and line 16 (Methods and Supplementary Information), which share the same lower hyperfine state. The respective upper hyperfine states have the same particle spin coupling but differ in the coupling between total particle spin and rotational angular momentum. This results in different total angular momenta F' in the upper states. For maximum resolution we address individual Zeeman components of the spin structure of the vibrational transition in the presence of a small magnetic field. We specifically measure the $m_F = 0 \rightarrow m'_F = 0$ Zeeman components, because they exhibit only a comparatively small quadratic Zeeman shift (Methods). Here, m_F (m'_F) is the projection of the total angular momentum F (F') on the static magnetic field direction.

Figure 3 shows one Zeeman component of line 12 and of line 16. The highest line resolutions obtained were 3×10^{11} (full linewidths smaller than 0.2 kHz). We measured several systematic shifts. The first is the Zeeman shift, for which we measured the transition

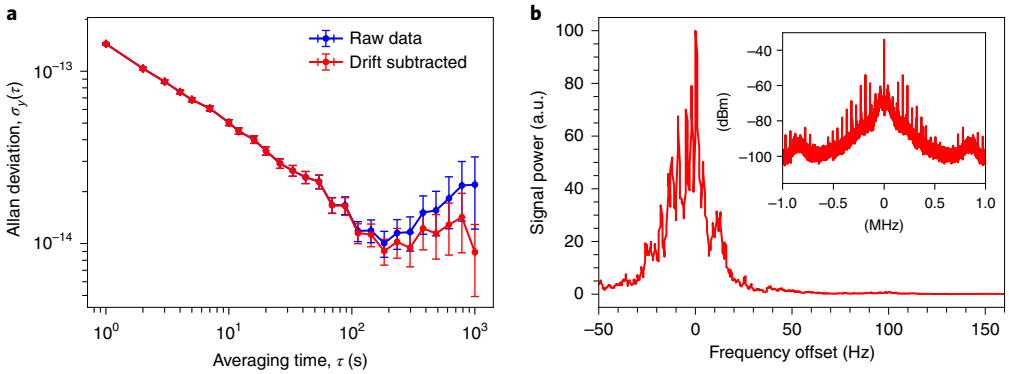

Fig. 2 | Spectral properties of the mid-infrared laser source. a, Fractional Allan deviation of the computed frequency value of the 5.1 μm radiation. The error bars for the Allan deviation are estimated as 68% confidence intervals. **b**, The heterodyne beat between a mode of the optically stabilized frequency comb and an independent frequency-stable 1.5 μm laser (not shown in Fig. 1). Averaging time: 1.5 min. Inset: beat on a larger frequency scale. The observed linewidth of less than 50 Hz, together with other data (Methods), indicate that the mid-infrared radiation has a linewidth of similiar value.

frequency of each line for three values of the magnetic field $B<1$ G. The shifts are consistent with the ab initio prediction. Assuming the predicted quadratic-in-B scaling, an extrapolation to $B=0$ was performed. Second, the laser light for beryllium ion laser cooling (0.2–0.5 mW at 313 nm) potentially causes a light shift via the polarizability of the molecular ion. Measurement showed that there is no effect at the level of 0.2 kHz, and the theoretical estimate justifies setting this shift to zero in our analysis. The third shift is caused by the trap radiofrequency (RF) electric field. Measurement of the transition frequency of each line for three RF amplitude values allowed for an extrapolation to zero amplitude. The extrapolated values are ~0.3 kHz smaller than the values at our nominal operational RF amplitude. Fourth, we irradiate the spectroscopy wave and the two photodissociation lasers alternately to avoid light shifts caused by the latter. Fifth, our theoretical estimation reveals that other systematic shifts are negligible compared to the uncertainties resulting from the above determinations. Further details are provided in the Methods.

We obtain the extrapolated zero-field frequencies

$$\begin{aligned} f_{12}^{(\mathrm{exp})} &= 58,605,013,478.03(19)_{\mathrm{exp}}\ \mathrm{kHz} \\ f_{16}^{(\mathrm{exp})} &= 58,605,054,772.08(26)_{\mathrm{exp}}\ \mathrm{kHz} \end{aligned} \quad (1)$$

The indicated uncertainties result from the realized linewidths and the achieved precision of the determination of the systematic shifts. Thus, the lowest experimental uncertainty is 3.3×10^{-12} fractionally.

The difference of the frequencies in equation (1) is a spin–rotation splitting. Its experimental value can be compared with the predicted splitting (equation (9), Methods). Theory and experiment agree very well within the combined uncertainty of 0.54 kHz.

We also compare the above values with ab initio values $f_i^{(\mathrm{theor})}$, computed using the approach described in the Methods. Using 2018 Committee on Data for Science and Technology (CODATA 2018) values for the fundamental constants[23] and their uncertainties (case I) results in

$$\begin{aligned} f_{12}^{(\mathrm{theor})} &= \\ &58,605,013,477.8(5)_{\mathrm{theor,QED}}(8)_{\mathrm{theor,spin}}(13)_{\mathrm{CODATA2018}}\ \mathrm{kHz} \\ f_{16}^{(\mathrm{theor})} &= \\ &58,605,054,771.6(5)_{\mathrm{theor,QED}}(9)_{\mathrm{theor,spin}}(13)_{\mathrm{CODATA2018}}\ \mathrm{kHz} \end{aligned} \quad (2)$$

For both frequencies, the indicated uncertainties are (0.8, 1.5, 2.2)$\times10^{-11}$ in fractional terms. The first uncertainty of both frequencies, 0.5 kHz, is an estimate of the unevaluated quantum electrodynamics (QED) contributions. It has been reduced by a factor of 42 in theoretical work spanning the past nine years. If, for m_e, m_p, m_d, the most accurate Penning trap mass values[24–26] are used (case II), instead of their CODATA 2018 values, the predictions are shifted by +1.5 kHz, and the last uncertainty contribution reduces to 1.1 kHz. Our experimental values are consistent with both predictions I and II within the combined uncertainties.

Any normalized linear combination of the two experimental vibrational frequencies, with respective theoretical spin structure contributions subtracted, yields the spin-averaged vibrational frequency

$$f_{\mathrm{spin\text{-}avg}}^{(\mathrm{exp})} = b_{12}(f_{12}^{(\mathrm{exp})} - f_{\mathrm{spin},12}^{(\mathrm{theor})}) + (1-b_{12})(f_{16}^{(\mathrm{exp})} - f_{\mathrm{spin},16}^{(\mathrm{theor})}) \quad (3)$$

We may choose the weight b_{12} in this composite frequency so that the total spin theory uncertainty is minimized[13]. However, we find that the uncertainty is minimized over a wide range of b_{12} values between 0 and 1, without any substantial reduction compared to that of $f_{\mathrm{spin},12}^{(\mathrm{theor})}$ and $f_{\mathrm{spin},16}^{(\mathrm{theor})}$. For $b_{12}\simeq0.5$:

$$f_{\mathrm{spin\text{-}avg}}^{(\mathrm{exp})} = 58,605,052,164.24(16)_{\mathrm{exp}}(85)_{\mathrm{theor,spin}}\ \mathrm{kHz} \quad (4)$$

The value $f_{\mathrm{spin\text{-}avg}}^{(\mathrm{exp})}$ agrees with the prediction $f_{\mathrm{spin\text{-}avg}}^{(\mathrm{theor})}$, equation (7), for both case I and II. The combined uncertainty of experimental and predicted values is 2.9×10^{-11}. This realizes a test of three-body quantum physics with state-of-the-art precision and limited by the uncertainties of the mass values.

The fundamental vibrational frequency $f_{\mathrm{spin\text{-}avg}}^{\mathrm{theor}}$ depends on the nuclear masses dominantly via the reduced nuclear mass $\mu=m_pm_d/(m_p+m_d)$, being closely proportional to $R_\infty\sqrt{\mu/m_e}$. We may therefore determine the ratio μ/m_e by requiring $f_{\mathrm{spin\text{-}avg}}^{(\mathrm{theor})}(\mu/m_e) = f_{\mathrm{spin\text{-}avg}}^{(\mathrm{exp})}$:

$$\begin{aligned} &\mu/m_e = \\ &1,223.899228668(7)_{\mathrm{exp}}(20)_{\mathrm{theor,QED}}(37)_{\mathrm{theor,spin}}(3)_{\mathrm{CODATA2018}} \end{aligned} \quad (5)$$

The last uncertainty contribution is due to that of the nuclear charge radii and the Rydberg constant R_∞, and the total fractional uncertainty is $u_r=3.5\times10^{-11}$. As shown in Fig. 4, the value equation (5) is consistent with the values from (1) CODATA 2018, (2) recent Penning trap measurements of m_e, m_p, m_d and m_d/m_p

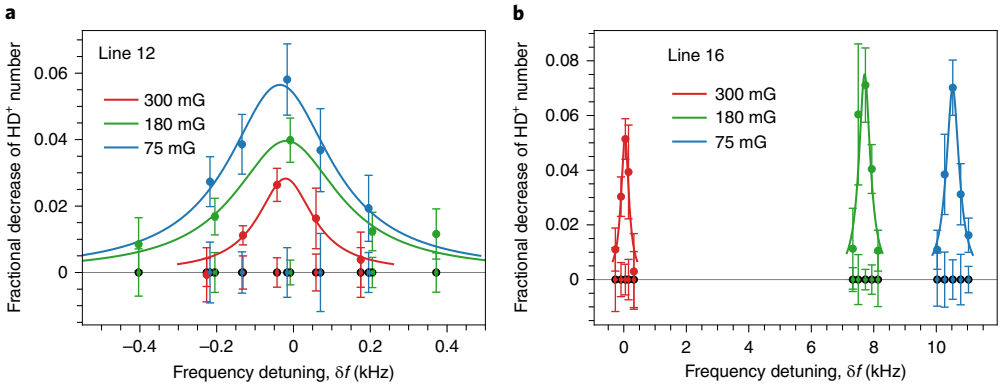

Fig. 3 | Two hyperfine components of the fundamental rovibrational transition of HD^+, at a frequency of 58.6 THz. a,**b**, Two Zeeman components ($v = 0,\ N = 0,\ F = 2,\ m_F = 0$) → ($v' = 1,\ N' = 0,\ F' = 1,\ m'_F = 0$) (line 12, **a**) and ($v = 0,\ N = 0,\ F = 2,\ m_F = 0$) → ($v' = 1,\ N' = 1,\ F' = 3,\ m'_F = 0$) (line 16, **b**), each for three values of the applied magnetic field. The quadratic Zeeman shift is evident on line 16, but it is not resolved on line 12. For line 16 at the lowest magnetic field setting, the line also contains the two transitions between stretched states ($m_F = \pm 2 \rightarrow m'_F = \pm 3$). For each indicated detuning δf of the laser frequency, two sets of measurements of HD^+ number decay were performed: with (coloured circles) and without (background decay, coloured circles outlined in black) application of spectroscopy radiation. From the mean of each set, the background decay mean was subtracted. The zero detuning frequency is arbitrary. The linewidths are due to a combination of power broadening and spectroscopy wave linewidth. The theoretical value for the natural linewidth of the transition is ~3 Hz. The lines are Lorentzian fits. Each error bar represents the standard deviation of the mean. The red data points and the fit for line 12 have been shifted by 0.17 kHz for clarity.

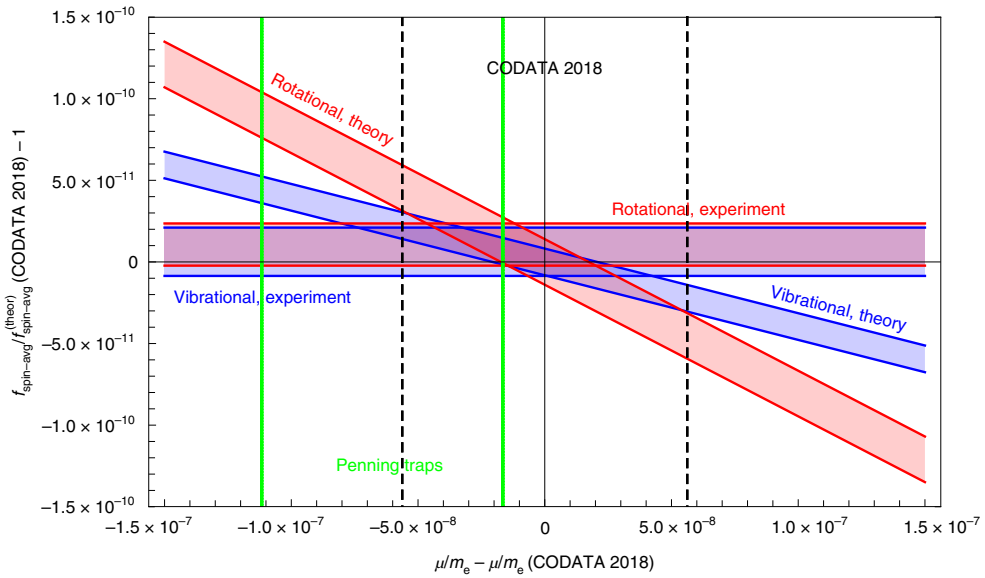

Fig. 4 | Determinations of the ratio of reduced nuclear mass to electron mass $\mu/m_e = m_e^{-1}m_p m_d/(m_p + m_d) \simeq 1,223.9$. Theoretical predictions (tilted bands) and experimental results (horizontal bands; independent of μ/m_e) are compared. Blue, this work; red, rotational transition[13]. The widths of the bands represent twice the uncertainties. For the prediction bands, the uncertainty includes the uncertainties of ab initio theory and the CODATA 2018 uncertainties of the fundamental constants, excluding μ/m_e. For the experimental bands, the uncertainties include the uncertainties of the experiment and of the spin contribution correction (equation (3)). For the rotational transition measurement, the latter is negligible. Black dashed line: CODATA 2018 $\pm 1\sigma$ uncertainty range. Green line: $\pm 1\sigma$ uncertainty range for the value μ/m_e computed from the results of refs. [24–26].

(refs. [25–28]) and (3) our HD^+ experimental rotational frequency and its theory[13]. The consistency between our vibrational and rotational values represents a direct test of the correctness of our QED and spin theory for this molecule, where today's uncertainties of the fundamental constants do not enter at a relevant level.

Because the CODATA uncertainty of $\mu_p = m_p/m_e$ contributes most to the CODATA 2018 uncertainty of $f^{(\text{theor})}_{\text{spin-avg}}$, we may alternatively fit m_p/m_e. In this case, for m_d/m_p we use the mean of the two recent precise values measured with Penning traps[26,28]. For the remaining fundamental constants we use the CODATA 2018 values. We obtain

$$m_p/m_e = 1,836.152673384(11)_{\text{exp}}(31)_{\text{theor,QED}}(55)_{\text{theor,spin}}(12)_{\text{CODATA2018,Fink}} \quad (6)$$

with total fractional uncertainty $u_r = 3.5 \times 10^{-11}$. The value is in agreement with other recent precision measurements:

(1) $1,836.152673374(78)_{exp}$, obtained from Penning trap determinations[24,25]
(2) $1,836.152673449(24)_{exp}(25)_{theor,QED}(13)_{CODATA2018,Fink}$ obtained from combining rotational spectroscopy of HD^+ and one Penning trap measurement of m_d/m_p (ref. [28])
(3) 1,836.152673349(71) obtained from a HD^+ vibrational overtone frequency, its theory and CODATA 2018 constants[16].

We note that our result, equation (6), is limited in precision by hyperfine structure theory. In the future, this limitation may be overcome by an improved theory[29].

In conclusion, we have demonstrated a one-photon optical spectroscopy method for ensembles of molecular ions that has achieved a more than 10^4 higher fractional resolution[30] and 400-fold higher fractional accuracy than previously demonstrated[30,31]. We have improved the absolute accuracy in determining a molecular-ion hyperfine splitting by optical spectroscopy by a factor of 400. We have also achieved an uncertainty of 3.3×10^{-12} in the experimental determination of a vibrational transition frequency of the present test ion, by measurement and theoretical evaluation of the systematic shifts. Because the employed test molecule is not particularly insensitive to external perturbations, we expect that similar (10^{-12}) inaccuracy levels should be achievable for numerous other molecular ion species. An independent test of the accuracy was possible by comparing our experimental composite transition frequency with the ab initio calculation. We found agreement at the 2.9×10^{-11} level. We have also shown the usefulness of the technique for the field of precision physics, by deriving values of fundamental mass ratios with uncertainties close to those of the most precise measurements[13,16,25,27]. A possible further exploitation of the technique is the study of molecular ions for tests of the equivalence principle[32]. We believe that the present technique is applicable also to electric quadrupole vibrational transitions of homonuclear diatomic ions[33], which are relevant for the above studies[34,35].

Although we have employed a light coolant atomic ion in the present demonstration, coolant atomic ions of larger mass are suitable for co-trapping and sympathetic cooling molecular ions of correspondingly larger mass. Notwithstanding a coolant ion mass upper bound of 160 u, a vast variety of singly charged molecular ions can be covered. The experimental configuration and employed techniques are comparatively accessible and should lend themselves to adoption by the spectroscopy community. Future work will explore the resolution and accuracy limits of this technique, as well as its applicability to single-species ensembles.

Online content

Any methods, additional references, Nature Research reporting summaries, source data, extended data, supplementary information, acknowledgements, peer review information; details of author contributions and competing interests; and statements of data and code availability are available at https://doi.org/10.1038/s41567-020-01150-7.

Received: 29 July 2020; Accepted: 14 December 2020;
Published online: 18 February 2021

References

1. Rosenband, T. et al. Observation of the $^1S_0 \rightarrow {}^3P_0$ clock transition in $^{27}Al^+$. *Phys. Rev. Lett.* **98**, 220801 (2007).
2. Chou, C. W., Hume, D. B., Thorpe, M. J., Wineland, D. J. & Rosenband, T. Quantum coherence between two atoms beyond $Q = 10^{15}$. *Phys. Rev. Lett.* **106**, 160801 (2011).
3. Dicke, R. H. The effect of collisions upon the Doppler width of spectral lines. *Phys. Rev.* **89**, 472–473 (1953).
4. Major, F. G. & Werth, G. High-resolution magnetic hyperfine resonance in harmonically bound ground-state ^{199}Hg ions. *Phys. Rev. Lett.* **30**, 1155–1158 (1973).
5. Rosenband, T. et al. Frequency ratio of Al^+ and Hg^+ single-ion optical clocks; metrology at the 17th decimal place. *Science* **319**, 1808–1812 (2008).
6. Derevianko, A. & Katori, H. Colloquium: Physics of optical lattice clocks. *Rev. Mod. Phys.* **83**, 331–347 (2011).
7. Poli, N., Oates, C. W., Gill, P. & Tino, G. M. Optical atomic clocks. *Riv. Nuovo Cim.* **36**, 555–624 (2013).
8. Ludlow, A. D., Boyd, M. M., Ye, J., Peik, E. & Schmidt, P. O. Optical atomic clocks. *Rev. Mod. Phys.* **87**, 637–701 (2015).
9. Diedrich, F., Bergquist, J. C., Itano, W. M. & Wineland, D. J. Laser cooling to the zero-point energy of motion. *Phys. Rev. Lett.* **62**, 403–406 (1989).
10. Lechner, R. et al. Electromagnetically-induced-transparency ground-state cooling of long ion strings. *Phys. Rev. A* **93**, 053401 (2016).
11. Schmidt, P. O. et al. Spectroscopy using quantum logic. *Science* **309**, 749–752 (2005).
12. Alighanbari, S., Hansen, M. G., Korobov, V. I. & Schiller, S. Rotational spectroscopy of cold and trapped molecular ions in the Lamb–Dicke regime. *Nat. Phys.* **14**, 555–559 (2018).
13. Alighanbari, S., Giri, G. S., Constantin, F. L., Korobov, V. I. & Schiller, S. Precise test of quantum electrodynamics and determination of fundamental constants with HD^+ ions. *Nature* **581**, 152–158 (2020).
14. Chou, C. W. et al. Frequency-comb spectroscopy on pure quantum states of a single molecular ion. *Science* **367**, 1458–1461 (2020).
15. Kondov, S. S. et al. Molecular lattice clock with long vibrational coherence. *Nat. Phys.* **15**, 1118–1122 (2019).
16. Patra, S. et al. Proton–electron mass ratio from laser spectroscopy of HD^+ at the part-per-trillion level. *Science* **369**, 1238–1241 (2020).
17. Wolf, F. et al. Non-destructive state detection for quantum logic spectroscopy of molecular ions. *Nature* **530**, 457–460 (2016).
18. Zhang, C. *Production and Sympathetic Cooling of Complex Molecular Ions*. PhD thesis, Heinrich-Heine-Universität Düsseldorf (2008).
19. Lakkaraju, H. S. & Schuessler, H. A. Motional side-band resonances in the microwave spectrum of stored ions. *J. Appl. Phys.* **53**, 3967–3974 (1982).
20. Cutler, L. S., Giffard, R. P. & McGuire, M. D. Thermalization of ^{199}Hg ion macromotion by a light background gas in an RF quadrupole trap. *Appl. Phys. B* **36**, 137–142 (1985).
21. Prestage, J. D., Tjoelker, R. L., Dick, G. J. & Maleki, L. Ultrastable Hg^+. *J. Mod. Opt.* **39**, 221–232 (1992).
22. Fisk, P. T. H., Sellars, M. J., Lawn, M. A. & Coles, C. Accurate measurement of the 12.6-GHz 'clock' transition in trapped Yb^+ ions. *IEEE Trans. Ultrason. Ferroelectr. Freq. Control* **44**, 344–354 (1997).
23. Tiesinga, E., Mohr, P. J., Newell, D. B. & Taylor, B. N. *Values of Fundamental Physical Constants* (2019); https://physics.nist.gov/cuu/Constants/index.html
24. Köhler, F. et al. The electron mass from *g*-factor measurements on hydrogen-like carbon $^{12}C^{5+}$. *J. Phys. B* **48**, 144032 (2015).
25. Heiße, F. et al. High-precision mass spectrometer for light ions. *Phys. Rev. A* **100**, 022518 (2019).
26. Rau, S. et al. Penning trap mass measurements of the deuteron and the HD^+ molecular ion. *Nature* **585**, 43–47 (2020).
27. Sturm, S. et al. High-precision measurement of the atomic mass of the electron. *Nature* **506**, 467–470 (2014).
28. Fink, D. J. & Myers, E. G. Deuteron-to-proton mass ratio from the cyclotron frequency ratio of H_2^+ to D^+ with H_2^+ in a resolved vibrational state. *Phys. Rev. Lett.* **124**, 013001 (2020).
29. Korobov, V. I., Karr, J.-Ph., Haidar, M. & Zhong, Z.-X. Hyperfine structure in the H_2^+ and HD^+ molecular ions at order $m\alpha^6$. *Phys. Rev. A* **102**, 022804 (2020).
30. Bressel, U. et al. Manipulation of individual hyperfine states in cold trapped molecular ions and application to HD^+ frequency metrology. *Phys. Rev. Lett.* **108**, 183003 (2012).
31. Biesheuvel, J. et al. High-precision spectroscopy of the HD^+ molecule at the 1-p.p.b. level. *Appl. Phys. B* **123**, 23 (2016).
32. Schiller, S. & Korobov, V. Test of time-dependence of the electron and nuclear masses with ultracold molecules. *Phys. Rev. A* **71**, 032505 (2005).
33. Germann, M., Tong, X. & Willitsch, S. Observation of dipole-forbidden transitions in sympathetically cooled, state-selected, homonuclear diatomic molecular ions. *Nat. Phys.* **10**, 820–824 (2014).
34. Schiller, S., Bakalov, D. & Korobov, V. I. Simplest molecules as candidates for precise optical clocks. *Phys. Rev. Lett.* **113**, 023004 (2014).
35. Karr, J.-Ph. H_2^+ and HD^+: candidates for a molecular clock. *J. Mol. Spectrosc.* **300**, 37–43 (2014).

Methods

Experimental apparatus. The ion trap apparatus used in the present work (Fig. 1) has been described previously[12,13]. The ion trap has a minimum distance between diagonally opposing electrodes of 8.6 mm. We have newly developed the laser system, which consists of two continuous-wave high-power diode lasers (L1, L2) emitting at 1.18 μm and 1.54 μm, whose radiation is mixed in a periodically poled $LiNbO_3$ crystal to produce a difference-frequency wave with a wavelength of 5.1 μm.

L1 and L2 are each phase-locked to a femtosecond fibre frequency comb, which is itself phase-locked to a 1.06 μm laser. We stabilize this laser to an ultra-low-expansion glass cavity[36], representing the optical flywheel reference of the whole system. Our phase-locking scheme allows flexible tuning of the mid-infrared radiation, limited by the tunability of the pump lasers.

The three optical beats required to implement the three phase locks are continuously monitored with spectrum analysers. The beats exhibit RF linewidths below 1 Hz. To independently verify the quality of the frequency comb stability, we show in Fig. 2 (right) the beat between a fourth diode laser (1.56 μm) stabilized to its own reference cavity[37] (neither are shown in Fig. 1) and an appropriate comb mode. This wavelength of 1.56 μm is notably different from the wavelength of the phase-locked comb mode, 1.06 μm, so the beat is a sensitive monitor of comb frequency noise. The full-width at half-maximum linewidth of the beat is less than 50 Hz. We infer that the linewidths of lasers L1 and L2 are also less than 50 Hz. The linewidth of the mid-infrared radiation is probably considerably less than 100 Hz because there is common-mode frequency noise in L1 and L2, originating from the frequency instability of the 1.06 μm laser.

We determine the absolute optical frequencies f_1 and f_2 of L1 and L2 in real time by measuring the repetition rate of the frequency comb and the carrier envelope offset frequency f_{ceo}. A GNSS-monitored hydrogen maser (H maser in Fig. 1) provides the reference frequency for the frequency counter. The frequency of the mid-infrared radiation is computed as $f_0 = f_1 - f_2$. Note that the value of f_{ceo} drops out of the difference frequency. The absolute frequency measurement uncovers the slow frequency drift of the mid-infrared radiation (of order 0.1 Hz min^{-1}). We take this into account during spectroscopy. The frequency instability of the mid-infrared radiation is less than 2×10^{-13} on timescales exceeding 1 s, and drops to below 2×10^{-14}. The maser frequency itself is measured by comparison with a one-pulse-per-second signal obtained from navigation satellites. The maser frequency's deviation from 10 MHz is corrected in the data analysis.

Experimental procedures. The preparation and spectroscopy sequence is a variation of a previously described procedure[13].

A destructive spectroscopy is performed, where the vibrationally excited molecular ions are subsequently dissociated by sequential excitation by two additional lasers (resonance-enhanced multiphoton dissociation, REMPD). The fractional decrease in the number of trapped, intact HD^+ ions is determined. The first laser for REMPD is a continuous-wave 1,475 nm laser tuned to the $(v'=1,\ N'=1)\rightarrow(v''=5,\ N''=2)$ transition, and the second one is a 266 nm continuous-wave laser for subsequent dissociation.

Before the spectroscopy wave irradiation we perform 40 s of rotational laser cooling to increase the population in the ground state ($v=0, N=0$).

An important difference compared to our previous work is that the spectroscopy radiation and the 1,475 nm and 266 nm waves for REMPD are not on simultaneously. Instead, we use a 5.2-s-long sequence during which spectroscopy and REMPD lasers are alternately blocked and unblocked for 100 ms each. Power broadening of the transition by the spectroscopy laser wave power is present but is kept moderate (Supplementary Fig. 2) by operating at sufficiently low power. However, performing spectroscopy with high laser power is helpful for finding transitions.

Vibrational transition. The HD^+ molecule harbours four angular momenta: electron spin, proton spin, deuteron spin and rotational angular momentum. The associated magnetic moments cause a hyperfine structure[38]. The ground rovibrational level has zero rotational angular momentum $N=0$, giving rise to four spin states with total angular momentum $F=0, 1, 2$ (these and other values are in part approximate quantum numbers). The first excited vibrational level $(v'=1,\ N'=1)$ has 10 spin states, with values $F'=0,\ 1,\ 2,\ 3$. Spin states are $(2F+1)$-fold degenerate in zero magnetic field. A small applied magnetic field leads to a quadratic Zeeman shift for $m_F=0$ states, a linear shift for the stretched states and a combined linear plus quadratic shift for the remaining Zeeman states.

We study two spin components having the same lower state (Supplementary Fig. 1):

line 12:

$$(v'=1,N'=1,G_1'=1,G_2'=2,F'=1)$$
$$\rightarrow(v'=1,N'=1,G_1'=1,G_2'=2,F'=1),$$

line 16:

$$(v=0,N=0,G_1=1,G_2=2,F=2)$$
$$\rightarrow(v'=1,N'=1,G_1'=1,G_2'=2,F'=3).$$

Here, G_1 refers to the sum of electron and proton spin, G_2 to the sum of G_1 and deuteron spin, and F to the sum of G_2 and rotational angular momentum N. We denote the transition frequencies in zero external fields by f_{12} and f_{16}.

Ab initio theory of the HD^+ vibrational transition. An ab initio transition frequency is composed of two contributions, $f_i^{(\mathrm{theor})} = f_{\mathrm{spin\text{-}avg}}^{(\mathrm{theor})} + f_{\mathrm{spin},i}^{(\mathrm{theor})}$. The main one is the spin-averaged frequency $f_{\mathrm{spin\text{-}avg}}^{(\mathrm{theor})}$, the difference between the level energies of the three-body system. The energies include the (essentially exactly calculated) non-relativistic energy plus relativistic, quantum-electrodynamic and finite-nuclear-size corrections evaluated by perturbation theory[39]. The calculated value is

$$f_{\mathrm{spin\text{-}avg}}^{(\mathrm{theor})} = 58,605,052,163.9(5)_{\mathrm{theor,QED}}(13)_{\mathrm{CODATA2018}}\ \mathrm{kHz}\ \ (\mathrm{case\ I}) \qquad (7)$$

CODATA 2018 values[23] of the fundamental constants have been used (case I), and the frequency value is updated compared to the value presented in ref. [40]. The contributions of relative order $(\alpha^0, \alpha^2, \alpha^3, \alpha^4, \alpha^5, \alpha^6)$ to equation (7) are (58,604,301,249.69, 1,003,554.55, −250,978.39, −1,770.95, 109.52, −0.77) kHz. The proton size contributes $-17.17(8)_{\mathrm{CODATA2018}}$ kHz, the deuteron size $-109.67(8)_{\mathrm{CODATA2018}}$ kHz; these contributions are included in the term of relative order α^2. Several further corrections were added, for example stemming from the polarizability of the deuteron, from second-order vibrational contributions (of relative order α^8) and so on, amounting to 0.26 kHz. The first uncertainty indicated in equation (7), $u(f_{\mathrm{spin\text{-}avg}}^{(\mathrm{theor})}) = 0.5\,\mathrm{kHz}$ (8×10^{-12} fractionally), is an estimate of the unevaluated QED contributions. The second uncertainty is due to the uncertainties of the fundamental constants. Here, the most important contribution is from the uncertainty of m_p/m_e, 1.1 kHz.

To obtain the functional dependence of the spin-averaged frequency on $\mu_p = m_p/m_e$ we calculated, ab initio, the derivative $\partial \ln f_{\mathrm{spin\text{-}avg}}^{(\mathrm{theor})}(\mu_p)/\partial \ln \mu_p|_{m_d/m_p=\mathrm{const.}} = -0.4846$, which is close to the Born–Oppenheimer value of $-\frac{1}{2}$.

The hyperfine structure in both the ground and excited vibrational level results in the hyperfine shifts $f_{\mathrm{spin},i}$. The main contribution to the hyperfine structure of each level comes from the Fermi contact interaction between electron spin and proton spin, followed by the contact interaction between the electron spin and the deuteron spin. These and further interactions are described by an effective Hamiltonian[38] and quantified by corresponding spin structure coefficients: $\mathcal{E}_4, \mathcal{E}_5$ for the $(v=0, N=0)$ level and $\mathcal{E}_1', \ldots, \mathcal{E}_9'$ for the $(v'=1, N'=1)$ level. The different strengths of the interactions in the two levels lead to a non-zero hyperfine shift. Given the aim of this work, it is important to have an accurate prediction for the hyperfine shift, implying the need for an accurate ab initio computation of the coefficients $\mathcal{E}_i$. A high-precision calculation[41] provides the set of Fermi contact interaction coefficients S_a: $(\mathcal{E}_4, \mathcal{E}_4', \mathcal{E}_5, \mathcal{E}_5')$. The values $\mathcal{E}_4, \mathcal{E}_5$ for the ground state $(v=0, N=0)$ have already played a role in rotational spectroscopy[13]. For the level $(v'=1, N'=1)$, $\mathcal{E}_4', \mathcal{E}_5'$ are computed here and are given in the Supplementary Information. These coefficients have fractional theoretical uncertainties, ϵ_F, of order α^3. We estimate $\epsilon_F = 1\times10^{-6}$. The set S_a contributes approximately $\delta_{S_a,i} = \epsilon_F(\gamma_{i,4}\mathcal{E}_4, \gamma_{i,4}'\mathcal{E}_4', \gamma_{i,5}'\mathcal{E}_5, \gamma_{i,5}'\mathcal{E}_5') \simeq (0.23, 0.23, 0.07, 0.07)\,\mathrm{kHz}$ to both $f_{\mathrm{spin},12}^{(\mathrm{theor})}$ and $f_{\mathrm{spin},16}^{(\mathrm{theor})}$. The sensitivities $\gamma_{i,k}, \gamma_{i,k}'$ are taken from Supplementary Table 1.

The coefficient $\mathcal{E}_1'$ is the next-largest spin coefficient. It has recently been the subject of intense theory work beyond the Breit–Pauli approximation, resulting in the value shown in Supplementary Table 1, with an improved theory uncertainty of $u_1' = 0.05\,\mathrm{kHz}$ (ref. [29] and Karr, J.-Ph. & Haidar, M., personal communication). The set S_b comprising the remaining spin coefficients, $\mathcal{E}_2', \mathcal{E}_3', \mathcal{E}_6', \mathcal{E}_7', \mathcal{E}_8', \mathcal{E}_9'$, has been computed within the Breit–Pauli approximation. It neglects terms of relative order α^2, so we assume that the fractional uncertainties of the set's elements are $\epsilon_0 = \alpha^2$. As a result, the dominant contributions of the set $(\mathcal{E}_1',\ S_b)$ to the uncertainties of $f_{\mathrm{spin},12}^{(\mathrm{theor})}$ and $f_{\mathrm{spin},16}^{(\mathrm{theor})}$ are from the coefficients $\mathcal{E}_7'$ and $\mathcal{E}_6'$, respectively.

In summary, the individual spin frequencies are

$$\begin{aligned} f_{\mathrm{spin},12}^{(\mathrm{theor})} &= -38,686.1(8)_{\mathrm{theor,spin}}\ \mathrm{kHz} \\ f_{\mathrm{spin},16}^{(\mathrm{theor})} &= 2,607.7(9)_{\mathrm{theor,spin}}\ \mathrm{kHz} \end{aligned} \qquad (8)$$

The uncertainties were estimated here as

$$u_{\mathrm{theor,spin}}(f_{\mathrm{spin},i}^{(\mathrm{theor})}) = |\gamma_{i,1}'u_1'| + \epsilon_0 \sum_{k=2,3,6,7,8,9} |\gamma_{i,k}'\mathcal{E}_k'| + \epsilon_F \sum_{k=4,5} |\gamma_{i,k}'\mathcal{E}_k'| + |\gamma_{i,k}\mathcal{E}_k|$$

The uncertainties from the various spin coefficients are not added quadratically because we cannot assume that they are independent random errors. The sum of equation (7) and equation (8) is equation (2).

The hyperfine splitting $f_{\mathrm{spin},16}^{(\mathrm{theor})} - f_{\mathrm{spin},12}^{(\mathrm{theor})}$ depends only on the spin coefficients of the upper level, because line 12 and line 16 have a common lower state. The uncertainty of the splitting is not affected by the uncertainties of $\mathcal{E}_4', \mathcal{E}_5'$ because $\gamma_{12,4}' = \gamma_{16,4}', \gamma_{12,5}' \approx \gamma_{16,5}'$. The uncertainty is mostly determined by the uncertainties of the next-next-largest coefficients $\mathcal{E}_6'$ and $\mathcal{E}_7'$:

$$f_{\mathrm{spin},16}^{(\mathrm{theor})} - f_{\mathrm{spin},12}^{(\mathrm{theor})} = 41,293.81(44)_{\mathrm{theor,spin}}\ \mathrm{kHz} \qquad (9)$$

The difference of the two measured vibrational frequencies is

$$f_{\mathrm{spin},16}^{(\mathrm{exp})} - f_{\mathrm{spin},12}^{(\mathrm{exp})} = 41,294.06(32)_{\mathrm{exp}}\ \mathrm{kHz}$$

in very good agreement with the prediction.

Systematic shifts. We have previously computed several external-field shifts of vibrational transition frequencies: Zeeman shift[42], electric quadrupole shift[43], d.c. Stark shift, black-body radiation shift, and spin-state dependence of the d.c. Stark and light shift[44]. The black-body radiation shift and electric quadrupole shift are negligible.

The Zeeman shifts for the components $m_F = 0 \rightarrow m'_F = 0$ of line 12 and 16 are $-2.9\,\mathrm{kHz\,G^{-2}}$ and $-117\,\mathrm{kHz\,G^{-2}}$, respectively. For the transitions between stretched states, $m_F = \pm 2 \rightarrow m'_F = \pm 3$ of line 16, the Zeeman shift is purely linear, with coefficients $\mp 0.55\,\mathrm{kHz\,G^{-1}}$.

The light shift of the lower and upper vibrational levels due to the 313 nm cooling radiation can be computed using the ab initio frequency-dependent polarizability values. The latter can be calculated using the procedure described in ref. [44]. For the lower level, they have already been reported in ref. [13]. For the upper level, the scalar (s) and tensor (t) polarizabilities are $\alpha_s(v' = 1,\ N' = 1,\ \lambda = 313\ \mathrm{nm}) = 4.475$ atomic units, $\alpha_t(v' = 1,\ N' = 1,\ \lambda = 313\ \mathrm{nm}) = -1.442$ atomic units. They are within 1.5 atomic units of the values for the lower level. The calculated light shift is therefore negligible.

Following ref. [13], we also investigated the effect on the transition frequency of a substantial displacement of the atomic ion cluster in the radial direction. When this occurs, the HD^+ ion string does not visibly shift. The deformation was obtained by substantially changing the d.c. voltages on the two lower trap electrodes by 5 V, shifting the beryllium cluster by ~0.10 mm orthogonally to the trap axis. No frequency shift was observed, with an upper bound of 0.4 kHz (Supplementary Fig. 3). The upper bound of the corresponding frequency shift of the rotational transition[13] was substantially smaller than this value. We expect the shifts to be of similar absolute magnitude for the two cases. We therefore do not apply any correction or uncertainty for this perturbation in our analysis. Thus, the only systematic shifts corrected for in this work are Zeeman and trap-induced d.c. Stark shifts (see main text).

For every measured transition line we assigned one-half of the fitted full width as the statistical uncertainty of the line centre transition frequency.

Composite frequency. The spin theory uncertainty of the composite frequency is computed as

$$u_{\mathrm{theor,spin}}(f^{(\mathrm{exp})}_{\mathrm{spin\text{-}avg}}) = |\textstyle\sum_{i=12,16} b_i\gamma'_{i,1}u'_1| + \epsilon_0 \sum_{k=2,3,6,7,8,9} |\sum_{i=12,16} b_i\gamma'_{i,k}\mathcal{E}'_k| + \epsilon_F \sum_{k=4,5} (|\sum_{i=12,16} b_i\gamma'_{i,k}\mathcal{E}'_k| + |\sum_{i=12,16} b_i\gamma_{i,k}\mathcal{E}_k|)$$

where $b_{16} = 1 - b_{12}$.

Previous results on high-resolution spectroscopy and mid-infrared spectroscopy sources. We briefly review the work achieving the highest line resolutions without the Lamb–Dicke or resolved-carrier regime. For gas-phase neutral molecules at non-cryogenic temperature, line resolutions up to 9×10^{10} have been achieved for vibrational transitions[45–47] and 7×10^9 for electronic transitions[48], using saturation or Ramsey spectroscopy (for a special case, see ref. [49]). By contrast, for atomic and molecular ions under gaseous conditions, the best resolutions have been considerably lower. For example, saturation spectroscopy of gas-phase molecular ions has led to 2×10^6 resolution, with absolute full linewidths at the 50 MHz level[50]. Using the ion beam technique, electronic and vibrational transitions have been observed with resolutions up to 2.5×10^6 (ref. [51]) and 4×10^6 (refs. [52,53]), respectively. In ion traps equipped with cooling by collisions with cold helium buffer gas, a resolution of 3×10^6 in vibrational spectroscopy (30 MHz linewidth) has been reached[54].

Previously, one-photon vibrational spectroscopy of sympathetically cooled molecular ion ensembles has been reported[30,33,55–58]. However, in these experiments, the spectroscopy wave was irradiated along the trap axis and/or the laser linewidth was high, leading to a highest line resolution of 2×10^7 (3 MHz absolute linewidth)[30].

Difference-frequency sources for spectroscopy have been reported previously (see ref. [59] for an overview), but had larger linewidth and/or higher frequency instability than the present one, in addition to shorter wavelength. At 3.4 µm, linewidths of 60 kHz (ref. [60]) and more recently of 3.5 kHz (ref. [61]) were achieved. An alternative approach makes use of quantum cascade lasers. They have been shown to allow ultra-narrow linewidth and precise frequency calibration[62,63] (see ref. [64] for a review).

Data availability

Data that support the plots within this paper and other findings of this study are available from the corresponding author upon reasonable request. Source data are provided with this paper.

References

36. Wiens, E., Nevsky, A. Y. & Schiller, S. Resonator with ultrahigh length stability as a probe for equivalence-principle-violating physics. *Phys. Rev. Lett.* **117**, 271102 (2016).
37. Chen, Q.-F. et al. A compact, robust and transportable ultra-stable laser with a fractional frequency instability of 1×10^{-15}. *Rev. Sci. Instrum.* **85**, 113107 (2014).
38. Bakalov, D., Korobov, V. I. & Schiller, S. High-precision calculation of the hyperfine structure of the HD^+ ion. *Phys. Rev. Lett.* **97**, 243001 (2006).
39. Korobov, V. I., Hilico, L. & Karr, J.-Ph. Fundamental transitions and ionization energies of the hydrogen molecular ions with few ppt uncertainty. *Phys. Rev. Lett.* **118**, 233001 (2017).
40. Aznabayev, D. T., Bekbaev, A. K. & Korobov, V. I. Leading-order relativistic corrections to the rovibrational spectrum of H_2^+ and HD^+ molecular ions. *Phys. Rev. A* **99**, 012501 (2019).
41. Korobov, V. I., Koelemeij, J. C. J., Hilico, L. & Karr, J.-Ph. Theoretical hyperfine structure of the molecular hydrogen ion at the 1-ppm level. *Phys. Rev. Lett.* **116**, 053003 (2016).
42. Bakalov, D., Korobov, V. & Schiller, S. Magnetic field effects in the transitions of the HD^+ molecular ion and precision spectroscopy. *J. Phys. B* **44**, 025003 (2011).
43. Bakalov, D. & Schiller, S. The electric quadrupole moment of molecular hydrogen ions and their potential for a molecular ion clock. *Appl. Phys. B* **114**, 213–230 (2014).
44. Schiller, S., Bakalov, D., Bekbaev, A. K. & Korobov, V. I. Static and dynamic polarizability and the Stark and blackbody-radiation frequency shifts of the molecular hydrogen ions H_2^+, HD^+ and D_2^+. *Phys. Rev. A* **89**, 052521 (2014).
45. Hall, J. L., Bordé, C. J. & Uehara, K. Direct optical resolution of the recoil effect using saturated absorption spectroscopy. *Phys. Rev. Lett.* **37**, 1339–1342 (1976).
46. Salomon, C., Bréant, C., Bordé, C. & Barger, R. Ramsey fringes using transitions in the visible and 10-µm spectral regions—experimental methods. *J. Phys. Colloq.* **42**, 3–14 (1981).
47. Bagayev, S. N., Baklanov, A. E., Chebotayev, V. P. & Dychkov, A. S. Superhigh resolution spectroscopy in methane with cold molecules. *Appl. Phys. B* **48**, 31–35 (1989).
48. Cheng, W.-Y., Chen, L., Yoon, T. H., Hall, J. L. & Ye, J. Sub-doppler molecular-iodine transitions near the dissociation limit (523–498 nm). *Opt. Lett.* **27**, 571–573 (2002).
49. Bagayev, S. N. et al. Second-order doppler-free spectroscopy. *Appl. Phys. B* **52**, 63–66 (1991).
50. Markus, C. R., Kocheril, P. A. & McCall, B. J. Sub-doppler rovibrational spectroscopy of the ν_1 fundamental band of D_2H^+. *J. Mol. Spectrosc.* **355**, 8–13 (2019).
51. Mills, A. A. et al. Ultra-sensitive high-precision spectroscopy of a fast molecular ion beam. *J. Chem. Phys.* **135**, 224201 (2011).
52. Wing, W. H., Ruff, G. A., Lamb, W. E. & Spezeski, J. J. Observation of the infrared spectrum of the hydrogen molecular ion HD^+. *Phys. Rev. Lett.* **36**, 1488–1491 (1976).
53. Coe, J. V. et al. Sub-doppler direct infrared laser absorption spectroscopy in fast ion beams: the fluorine hyperfine structure of HF^+. *J. Chem. Phys.* **90**, 3893–3902 (1989).
54. Markus, C. R., Thorwirth, S., Asvany, O. & Schlemmer, S. High-resolution double resonance action spectroscopy in ion traps: vibrational and rotational fingerprints of $CH_2NH_2^+$. *Phys. Chem. Chem. Phys.* **21**, 26406–26412 (2019).
55. Roth, B., Koelemeij, J. C. J., Daerr, H. & Schiller, S. Rovibrational spectroscopy of trapped molecular hydrogen ions at millikelvin temperatures. *Phys. Rev. A* **74**, 040501 (2006).
56. Koelemeij, J. C. J., Noom, D. W. E., de Jong, D., Haddad, M. A. & Ubachs, W. Observation of the $v' = 8 \leftarrow v = 0$ vibrational overtone in cold trapped HD^+. *Appl. Phys. B* **107**, 1075–1085 (2012).
57. Biesheuvel, J. et al. Probing QED and fundamental constants through laser spectroscopy of vibrational transitions in HD^+. *Nat. Commun.* **7**, 10385 (2016).
58. Calvin, A. T. et al. Rovibronic spectroscopy of sympathetically cooled $^{40}CaH^+$. *J. Phys. Chem. A* **122**, 3177–3181 (2018).
59. Liao, C.-C., Lien, Y.-H., Wu, K.-Y., Lin, Y.-R. & Shy, J.-T. Widely tunable difference frequency generation source for high-precision mid-infrared spectroscopy. *Opt. Express* **21**, 9238–9246 (2013).
60. Takahata, K. et al. Absolute frequency measurement of sub-doppler molecular lines using a 3.4-µm difference-frequency-generation spectrometer and a fiber-based frequency comb. *Phys. Rev. A* **80**, 032518 (2009).
61. Sera, H. et al. Sub-doppler resolution mid-infrared spectroscopy using a difference-frequency-generation source spectrally narrowed by laser linewidth transfer. *Opt. Lett.* **40**, 5467–5470 (2015).
62. Hansen, M. G., Magoulakis, E., Chen, Q.-F., Ernsting, I. & Schiller, S. Quantum cascade laser-based mid-IR frequency metrology system with ultra-narrow linewidth and 1×10^{-13}-level frequency instability. *Opt. Lett.* **40**, 2289–2292 (2015).
63. Argence, B. et al. Quantum cascade laser frequency stabilization at the sub-Hz level. *Nat. Photon.* **9**, 456–460 (2015).
64. Borri, S. et al. High-precision molecular spectroscopy in the mid-infrared using quantum cascade lasers. *Appl. Phys. B* **125**, 18 (2019).

Acknowledgements

We are indebted to E. Wiens for assistance with the frequency comb measurements. We are very grateful to J.-Ph. Karr for communicating the value of $\mathcal{E}_1'$ before publication. This work has received funding from the European Research Council (ERC) under the European Union's Horizon 2020 research and innovation programme (grant no. 786306, 'PREMOL'), from the Deutsche Forschungsgemeinschaft (Schi 431/23-1) and from both DFG and the state of Nordrhein-Westfalen via grant no. INST-208/737-1 FUGG. I.V.K. was partly supported by FP7-2013-ITN 'COMIQ' (grant no. 607491). V.I.K. acknowledges support from the Russian Foundation for Basic Research under grant no. 19-02-00058-a.

Author contributions

I.V.K., M.G.H. and S.S. developed the laser system. I.V.K., S.A. and G.S.G. performed the experiments and analysed the data. I.V.K., S.S. and V.I.K. performed theoretical calculations. S.S. conceived the study, supervised the work and wrote the manuscript. All authors contributed to editing of the manuscript.

Competing interests

The authors declare no competing interests.

Additional information

Supplementary information The online version contains supplementary material available at https://doi.org/10.1038/s41567-020-01150-7.

Correspondence and requests for materials should be addressed to S.S.

Peer review information *Nature Physics* thanks the anonymous reviewers for their contribution to the peer review of this work.

Reprints and permissions information is available at www.nature.com/reprints.

nature portfolio

https://doi.org/10.1038/s41567-020-01150-7

Supplementary information

Proton–electron mass ratio by high-resolution optical spectroscopy of ion ensembles in the resolved-carrier regime

In the format provided by the authors and unedited

Supplementary Information for "Proton-electron mass ratio by high-resolution optical spectroscopy of ion ensembles in the resolved-carrier regime"

I. Kortunov,[1] S. Alighanbari,[1] M. G. Hansen,[1] G. S. Giri,[1] V. I. Korobov,[2] and S. Schiller[1,*]

[1] *Institut für Experimentalphysik, Heinrich-Heine-Universität Düsseldorf, 40225 Düsseldorf, Germany*

[2] *Bogoliubov Laboratory of Theoretical Physics, Joint Institute for Nuclear Research, 141980 Dubna, Russia*

[*] Corresponding Author, e-mail: step.schiller@hhu.de

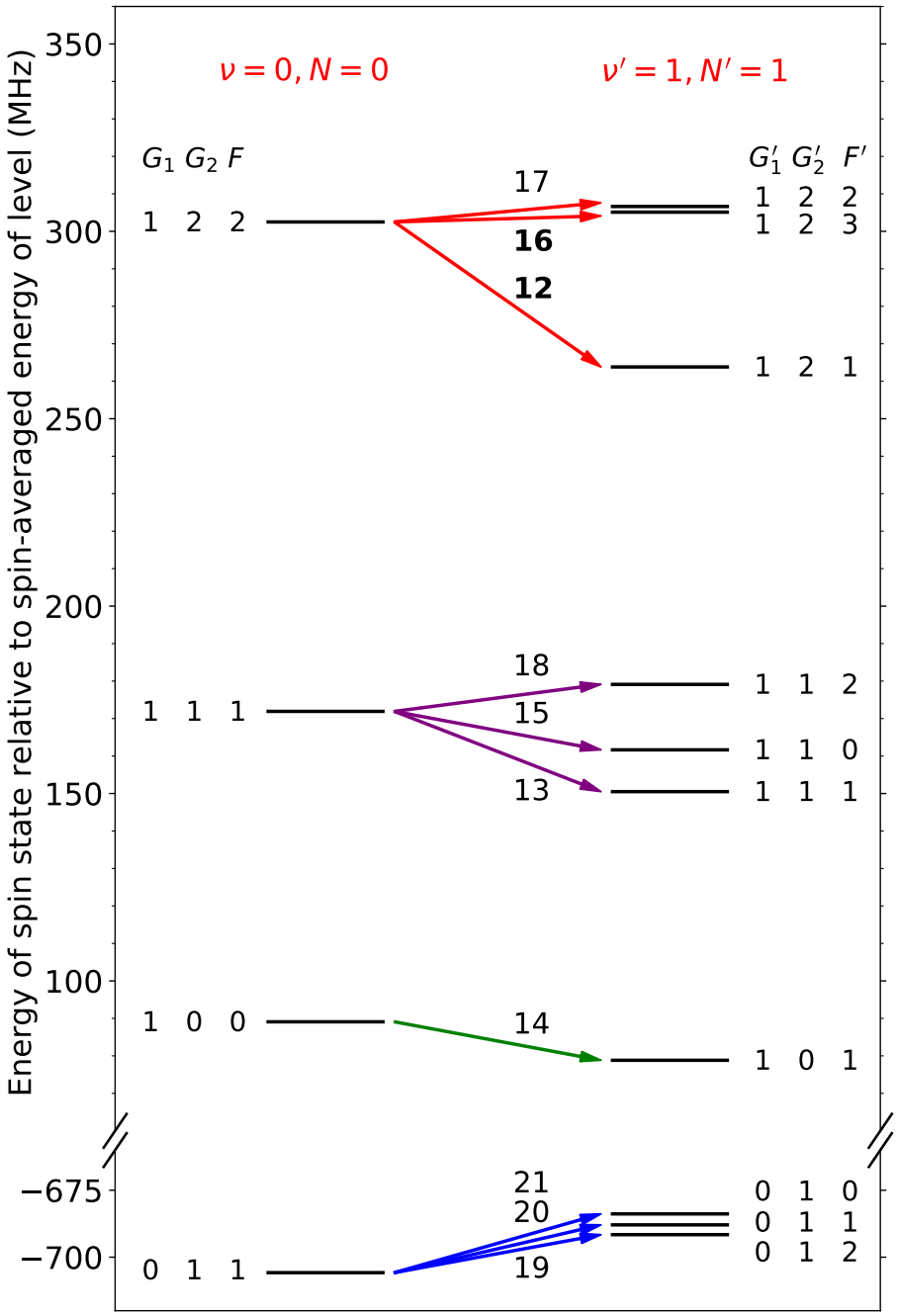

Supplementary Figure 1. **Hyperfine structure energy levels of HD^+ in the two relevant levels.** Shown are the ground vibrational level ($v = 0, N = 0$) (left) and the first excited vibrational level ($v' = 1, N' = 1$) (right) of the $^2\Sigma_g^+$ electronic state. The numbers next to the arrows indicate the line numbers. In this work, lines 12 and 16 were detected and measured.

		$\mathcal{E}'_1$	$\mathcal{E}'_2$	$\mathcal{E}'_3$	$\mathcal{E}'_4$	$\mathcal{E}'_5$	$\mathcal{E}'_6$	$\mathcal{E}'_7$	$\mathcal{E}'_8$	$\mathcal{E}'_9$	$\mathcal{E}_4$	$\mathcal{E}_5$
		30.28083	-0.03046	-0.004664	903.36802	138.91049	8.13669	1.24894	-0.002945	0.005659	925.39588	142.28781
Line i	$f^{(\mathrm{theor})}_{\mathrm{spin},i}$	$\gamma'_{i,1}$	$\gamma'_{i,2}$	$\gamma'_{i,3}$	$\gamma'_{i,4}$	$\gamma'_{i,5}$	$\gamma'_{i,6}$	$\gamma'_{i,7}$	$\gamma'_{i,8}$	$\gamma'_{i,9}$	$\gamma_{i,4}$	$\gamma_{i,5}$
12	-38.68609	-0.575	-0.565	-1.715	0.250	0.430	-0.011	-3.369	-3.306	-2.909	0.250	0.500
16	2.60772	0.500	0.500	1.000	0.250	0.500	-0.500	-1.000	-1.000	-0.500	0.250	0.500

Supplementary Table 1. **Spin hamiltonian coefficients, spin structure frequencies, and spin frequency derivatives.** $\mathcal{E}'_k$ are the coefficients of the spin Hamiltonian [45] for the $(v' = 1, N' = 1)$ level, in MHz. $\mathcal{E}_k$ are the coefficients for the ro-vibrational ground state $(v = 0, N = 0)$, already reported in [13]. $f^{(\mathrm{theor})}_{\mathrm{spin}}$ is the theoretical spin structure frequency in MHz. γ are the dimensionless sensitivities of the spin structure frequencies to the various spin Hamiltonian coefficients. $\gamma'_{i,k} = \partial f^{(\mathrm{theor})}_{\mathrm{spin},i} / \partial \mathcal{E}'_k$ refers to the upper state, $\gamma_{i,k} = -\partial f^{(\mathrm{theor})}_{\mathrm{spin},i} / \partial \mathcal{E}_k$ to the lower state.

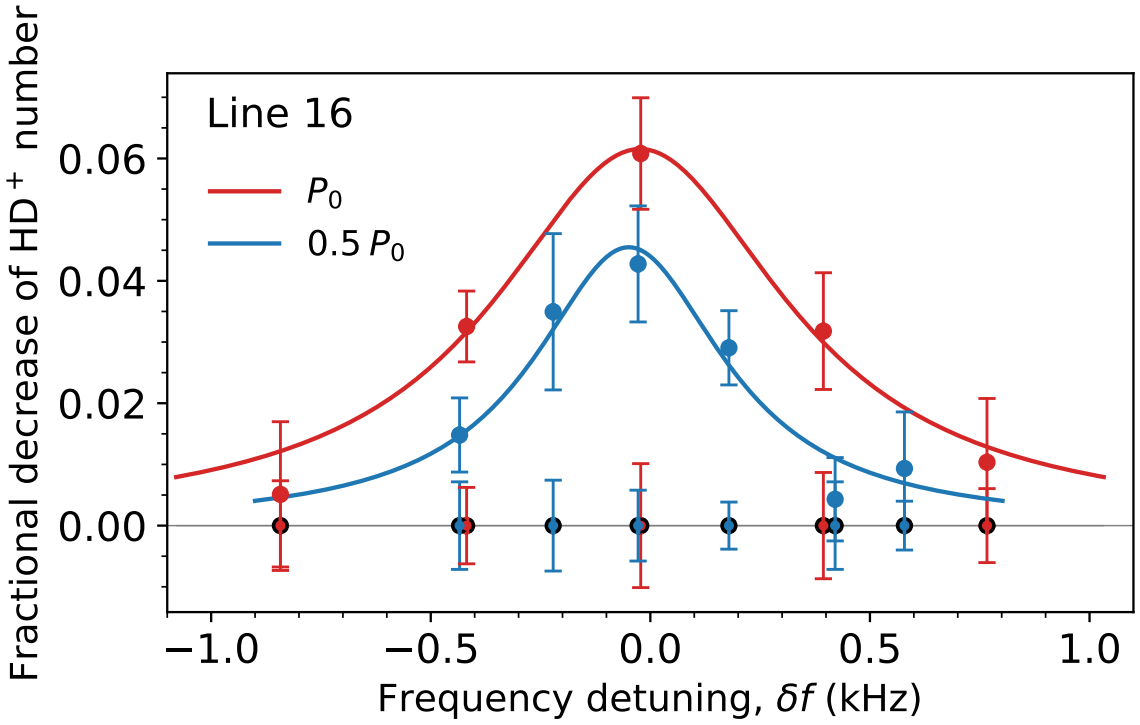

Supplementary Figure 2. **Power broadening of one Zeeman component of the vibrational transition.** The $m_F = 0 \rightarrow m'_F = 0$ component of line 16 was interrogated at two power settings of the 5.1 μm spectroscopy laser. Here, $B \simeq 0.6$ G. The zero of the frequency detuning is arbitrary. P_0 is the nominal power used in the measurements shown in the main text. Each error bar represents the standard deviation of the mean.

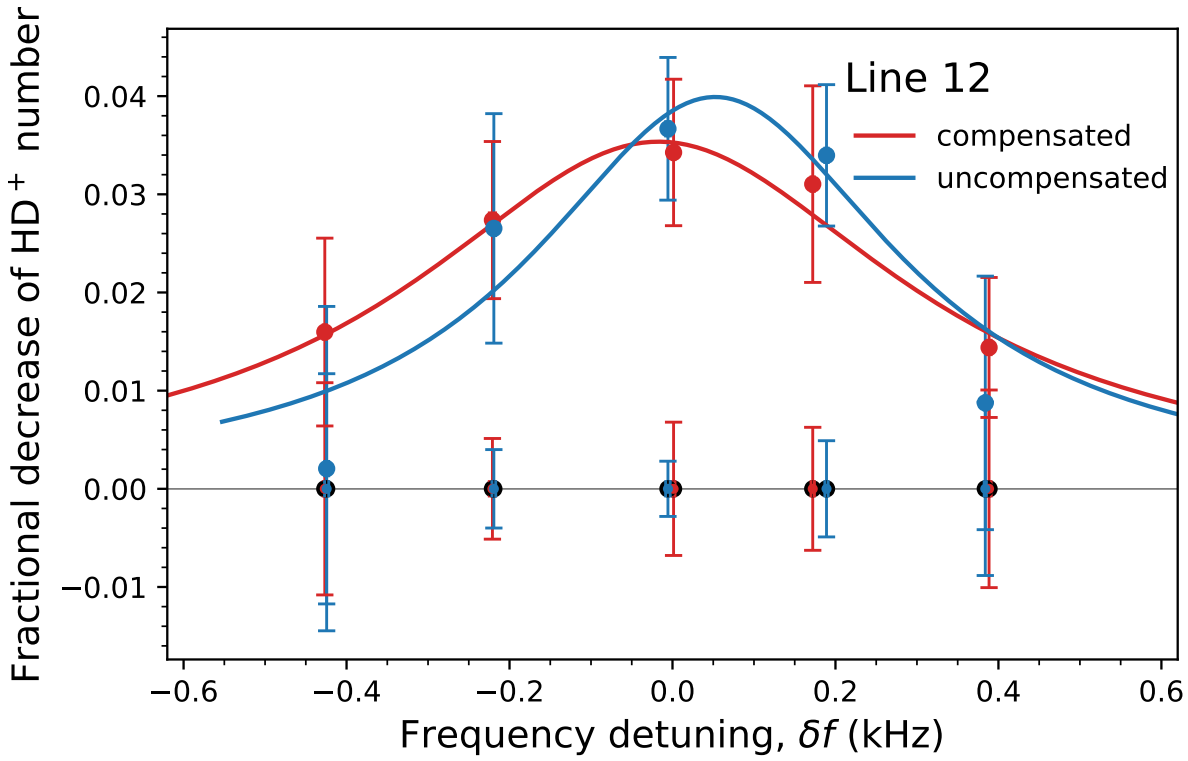

Supplementary Figure 3. **The effect of a displacement of the beryllium ion cluster from the trap axis.** One Zeeman component of the vibrational transition is measured with the beryllium ion cluster aligned with the trap axis (red) and with the cluster significantly shifted radially (blue). The $m_F = 0 \rightarrow m'_F = 0$ component of line 12 is shown. The zero of the frequency detuning is arbitrary. Each error bar represents the standard deviation of the mean.